Eur. Phys. J. E (2011) **34**: 81
DOI 10.1140/epje/i2011-11081-0

THE EUROPEAN PHYSICAL JOURNAL E

Regular Article

On the coalescence of sessile drops with miscible liquids

R. Borcia[a] and M. Bestehorn

Lehrstuhl Statistische Physik/Nichtlineare Dynamik, Brandenburgische Technische Universität, D-03046 Cottbus, Germany

Received 7 March 2011
Published online: 22 August 2011 –

Abstract. Sessile drops sitting on highly wettable solid substrates fuse in qualitatively different ways after contact, depending on the surface tension gradients between the mixing droplets. In early time evolution the drop coalescence can be fast or delayed (intermittent). In long time evolution a secondary drop formation can occur. We study numerically droplet dynamics during coalescence in two and three spatial dimensions, within a phase field approach. We discuss criteria to distinguish different coalescence regimes. A comparison with recent experiments will be done.

1 Introduction

Coalescence of liquid droplets is of great interest in the framework of micro-fluidic applications. For micro devices the coalescence becomes a very convenient solution to mix small portions of fluids in a controlled and reproducible way without power supply [1,2]. Drop coalescence through a planar interface has been frequently studied in the last decade both experimentally and numerically [3–6]. Depending on its impact velocity, the drop can fully merge into the liquid reservoir or can leave behind secondary (satellite) droplets. The parameters responsible for the formation of a daughter drop during the collision process were identified and widely discussed.

Coalescence of sessile droplets of the same liquid already provides challenging phenomena. Fusion process on substrates consists of two stages: an initial rapid growth of the meniscus bridge between the drops, and a slow rearrangement of the combined droplet shape from elliptical to a more circular shape at longer time. The time dependence of the width of the meniscus bridge between the two droplets was investigated in detail both experimentally and numerically [7–9]. For the coalescence of identical droplets, the separation line is straight. The bridge width becomes larger and larger in time, but the meniscus bridge remains always straight.

An even more interesting situation occurs when the fusing sessile drops have different surface tensions. In this case the coalescence is assisted by Marangoni effects at the droplet interfaces. Due to the flow from the droplet with lower surface tension to the droplet with higher surface tension the meniscus bridge between the interacting drops becomes curved. For small contact angles at the solid substrate, the lateral contact between approaching droplets is realized through the precursor liquid film at the solid substrate. Different behaviors can appear in early time evolution: a fast coalescence, when the connecting neck between the two drops fills up continuously, until the minimum of the liquid film between the interacting drops disappears and a delayed coalescence—called also intermittent coalescence—when the connecting film remains shallow, keeping the main droplet volumes separated for a longer time. The first experiments reporting delayed coalescence were performed in 1938 by D.H. Bangham and Z. Saweris [10]. In the last few years experimental investigations on this topic were recommenced qualitatively in [11] and quantitatively in [12,13]. In [12], the difference in surface tension has been identified as leading parameter for drop coalescence. It is shown that, for contact angles between 10° and 20°, a difference in surface tension between 3 and 5 mN/m leads to a rather sharp transition between the coalescence modes. Recently, theoretical tools able to describe delayed coalescence of droplets with different perfectly miscible liquids were proposed [14]. Two approaches were used to this aim: a lubrication approximation and a phase field model. Numerical simulations in two spatial dimensions clearly prove that the Marangoni stress makes an important contribution in different behaviors of droplets coalescence. The delay mechanism reduces to a problem of mass transport across a thin domain connecting two larger reservoirs. The two droplets with a body of different liquids are the reservoirs. The thin liquid channel connecting the reservoirs does not allow a rapid mixing of the two components of the two miscible liquids. Surface tension gradients (and, therefore, Marangoni flows) are maintained for some times between the droplets. The liquid exchange keeps the drops temporarily separated from each other and the two drops are running one after the other in the direction of the Marangoni flow.

The current paper is strongly motivated by very recent experimental facts which try to formulate a criterion for distinguishing between different coalescence modes [13].

[a] e-mail: borcia@physik.tu-cottbus.de

In this paper we study the droplet dynamics during the coalescence in two and three dimensions using phase field simulations. Beneath pattern formation, the shape of the flow field and concentration distributions are investigated in this paper. The geometry of the contact line between the two different fluids changes much from the 2D to 3D description and we try to answer the following questions: What is the influence of the third spatial dimension? What happens along 3D-contact lines? Do vortices or back flows exist? What is seen in the long time limit, fused or separated liquid portions?

The paper is organized as follows: sect. 2 presents the phase field model with the governing equations. Computer results in two and three spatial dimensions are reported and discussed in sect. 3. We gather the conclusions in sect. 4.

2 Equations

We consider two drops consisting of non-evaporative, perfectly miscible liquids, sitting on a solid substrate and surrounded by gas. In the current work, the phase field approach is utilized to describe the evolution of the multiphase system. The main idea underlying the phase field model is to introduce a variable which describes continuously the system. The most convenient phase field variable is the (scaled) density ρ. $\rho = 1$ designates the liquid phase (both liquids have the same density) and $\rho \approx 0$ the gas bulk. All the variables change strongly but continuously through the sharp interface. The position and the shape of the interface are tracked by using the density field. So, the multi-phase system is treated like an entire and the boundary conditions at the liquid-gas interfaces are eliminated. In the phase field formalism, the Navier-Stokes equations include phase field gradient terms for assuring the shear stress balance at the droplet interfaces [15–18]:

$$\rho \frac{\mathrm{d}\boldsymbol{v}}{\mathrm{d}t} = -\boldsymbol{\nabla} p + \rho \boldsymbol{\nabla} \left(\boldsymbol{\nabla} \cdot (\mathcal{K} \boldsymbol{\nabla} \rho) \right) + \boldsymbol{\nabla} \cdot \boldsymbol{\tau}. \tag{1}$$

In (1), p denotes the thermodynamical pressure $p(\rho) = \rho(\partial f/\partial \rho) - f$ with f as the free energy density for homogeneous phases. To account for the two stable states liquid and gaseous we chose [19]

$$f(\rho) \sim \rho^2 (\rho - 1)^2$$

and the control of the surface tension coefficient will be done through the gradient energy term $\mathcal{K}(\partial\rho/\partial z)^2/2$ ($\mathcal{K}$ is the gradient energy coefficient) [20]

$$\sigma = \int_{-\infty}^{+\infty} \mathcal{K} \left(\frac{\partial \rho}{\partial z} \right)^2 \mathrm{d}z.$$

The second term on the right-hand side in eq. (1) introduces the Korteweg interfacial stress, first introduced in [21] and later on studied by several authors (see [22–24] and references therein). This term includes the contribution of the capillary forces and may be extended by the part that includes concentration gradients. The two perfectly miscible liquids have to be distinguished by a second-order parameter—the molar fraction c. The molar fraction is $c = 1$ for the left droplet in fig. 1-a and $c = 0$ for the other one. Concentration gradients induce surface tension gradients. The Marangoni effect caused by surface tension difference between the two mixing liquids is taken into consideration in (1), assuming the parameter $\mathcal{K}$ depending linearly on c [25,26]

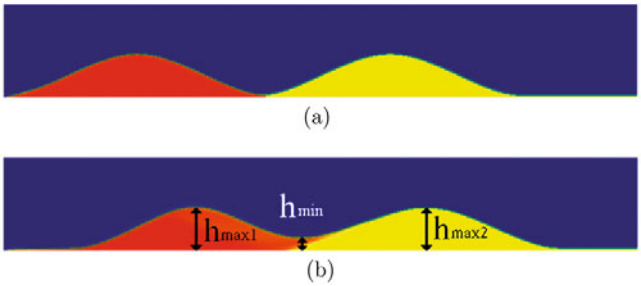

Fig. 1. (Color online) Sketch of the system. Two drops consisting of different perfectly miscible liquids are connected through a precursor film. An exchange of liquid appears through the bridging film induced by Marangoni driven flows: (a) $t = 0$; (b) $t \neq 0$.

$$\mathcal{K} = \mathcal{K}_0 - \mathcal{K}_C c \tag{2}$$

with $\mathcal{K}_0$ and $\mathcal{K}_C$ two material constants.

The third term on the right-hand side in eq. (1) introduces the viscous stress tensor $\boldsymbol{\tau}$

$$\boldsymbol{\tau} = \eta \left[\boldsymbol{\nabla} \otimes \boldsymbol{v} + (\boldsymbol{\nabla} \otimes \boldsymbol{v})^T - \frac{2}{3} (\boldsymbol{\nabla} \cdot \boldsymbol{v}) I \right],$$

where η represents the dynamic viscosity, the symbol $\otimes$ stands for the tensor product, the index T denotes the transposed, and I is the unit tensor.

The dynamics of the phase fields (ρ and c) is normally controlled by local conservation equations of the form

$$\frac{\partial \rho}{\partial t} = -\boldsymbol{\nabla} \cdot \boldsymbol{J}_\rho, \tag{3}$$

$$\frac{\partial (\rho c)}{\partial t} = -\boldsymbol{\nabla} \cdot \boldsymbol{J}_{\rho c}, \tag{4}$$

where $\boldsymbol{J}_\rho$ and $\boldsymbol{J}_{\rho c}$ are the mass and mass fraction fluxes, respectively,

$$\boldsymbol{J}_\rho = \rho \boldsymbol{v},$$
$$\boldsymbol{J}_{\rho c} = \rho c \boldsymbol{v} + D \boldsymbol{\nabla} (\rho c)$$

(D—the diffusion coefficient).

The full system of equations is complemented by boundary and initial conditions. The boundary conditions for the density field at the solid walls play an important role for the contact angle at the solid surface. In our model we control the contact angle through the density at the solid boundary ρ_S, a parameter describing the fluid-solid interactions. L. Pismen and Y. Pomeau [19] assume that

the only condition enforced on the solid surface (placed at $z = 0$) is

$$\rho = \rho_S. \tag{5}$$

A flat solid surface with variable wettability (and variable thickness of the precursor film) can be realized varying ρ_S in the range $0 < \rho_S < 1$. Large values for ρ_S correspond to small contact angles (and thin precursor films) and vice versa. In [19] an analytical formula is derived which relates the static contact angle θ to the solid density ρ_S

$$\cos\theta = -1 + 6\,\rho_S^2 - 4\,\rho_S^3, \tag{6}$$

numerically verified through phase field simulations [30]. So, with an appropriate choice of ρ_S ($\rho_S > 0.5$), one can simulate liquid droplets sitting on a hydrophilic surface under a given contact angle θ.

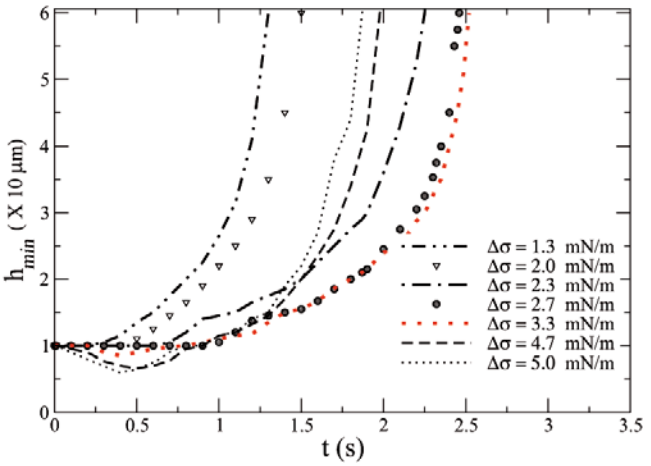

Fig. 2. (Color online) The minimal height of the bridging film between two interacting drops *versus* time for different surface tension gradients.

3 Numerical results

Equations (1), (3) and (4) are solved numerically in two and three spatial dimensions using a finite-difference method [27,28]. Similar computational codes were developed and validated earlier for 2D phase field models describing floating liquid droplets with applied temperature gradients [29], static [30] and dynamic contact angles of nearly circular drops running down on solid substrates under gravity effects [31].

3.1 Two-dimensional results

We assume two perfectly miscible liquid droplets of the same initial height $h(t = 0) = 0.1\,\mathrm{mm}$, the same density $\rho = 10^3\,\mathrm{kg/m^3}$, and the same kinematic viscosity $\nu = 5 \cdot 10^{-6}\,\mathrm{m^2/s}$ connected through a precursor film of order $10\,\mu\mathrm{m}$ (fig. 1-a). The two droplets are surrounded by a gas with $\rho_v \approx 1\,\mathrm{kg/m^3}$ and are sitting on a hydrophilic rigid surface (at $z = 0$) with $\rho_S = 0.95$. From (6) it follows a contact angle for both droplets of $\theta = 10°$. The simulations presented in this paragraph correspond to a mesh with 600×200 points. The system is confined in a box with no-slip conditions for the velocity field at the wall boundaries ($\boldsymbol{v} = 0$). The diffusion coefficient is $D = 10^{-9}\,\mathrm{m^2/s}$ in the liquid and $D = 0$ for the gas bulk. At the initial moment $t = 0$ the molar fraction is homogeneous in each drop with $c = 1$ for liquid 1 (left side in fig. 1-a) and $c = 0$ for liquid 2. In the gas atmosphere we consider also $c = 0$. According to the relation (2), a difference of surface tension appears between the two droplets if $\mathcal{K}_C \neq 0$. Drop 1 has the surface tension coefficient $\sigma_1 = 0.05\,\mathrm{N/m}$ and drop 2 has a higher surface tension. Owing to the surface tension difference, a surface flow occurs within the droplets from the left to the right pushing both drops to the right.

Recent experiments and simulations show modifications of the drop surface lateral profiles during the coalescence [12,14]. The Marangoni flow from one droplet to the other produces in the interacting region a decrease of the contact angle for drop 1 (with lower surface tension) and an increase of the contact angle for drop 2 (with higher surface tension). That can create a depression in the precursor film which could keep the droplets separated for some time. As an attempt to formulate a criterion to distinguish different coalescence regimes, we have represented the minimal height of the bridging film between drops h_{min} *versus* time t for different surface tension gradients (see fig. 2). One can observe that for $\Delta\sigma = \sigma_2 - \sigma_1 < 3.3\,\mathrm{mN/m}$, h_{min} increases monotonically with time. The connecting neck between the droplets is filled up continuously until complete fusion of the drops. This case is named "fast coalescence". For $\Delta\sigma \geq 3.3\,\mathrm{mN/m}$, h_{min} achieves a minimum in early time evolution. The droplets are in contact with each other, a liquid exchange occurs between the drops, the bridging film augments very slightly in vertical direction. The Marangoni flow from one liquid to the other causes an interruption in the growth of the connecting film after $\approx 0.4\,\mathrm{s}$. This situation is called "delayed" or "intermittent coalescence". The curve corresponding to $\Delta\sigma = 3.3\,\mathrm{mN/m}$ in fig. 2 designates the critical curve which separates the two coalescence regimes.

Experimentally it is difficult to reproduce initial conditions with exactly the same drop sizes. In order to compare our numerical results quantitatively with the experiments, we introduce a scaled parameter, called the coalescence coefficient:

$$\kappa = \frac{h_{min}}{h_{max1} - h_{min}}$$

(h_{max1} represents the height of the drop with lower surface tension, on the left side in fig. 1-b) and we trace κ over time t for different surface tension gradients between the drops (fig. 3). For one of the cases presented in fig. 3, we display also time series illustrating droplet patterns, concentration and flow fields during the coalescence. Concentration and flow distributions depicted in fig. 4 are relevant for all the situations described in figs. 2 and 3, respectively. The two components mix, a Marangoni flow

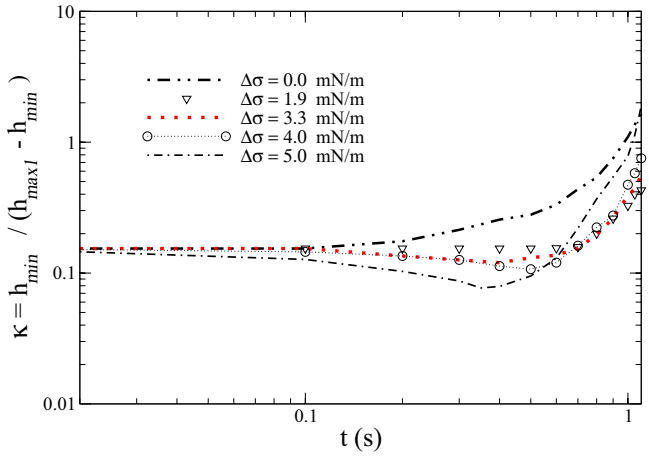

Fig. 3. (Color online) Coalescence coefficient over time for different surface tension gradients. The results are provided by two-dimensional phase field simulations.

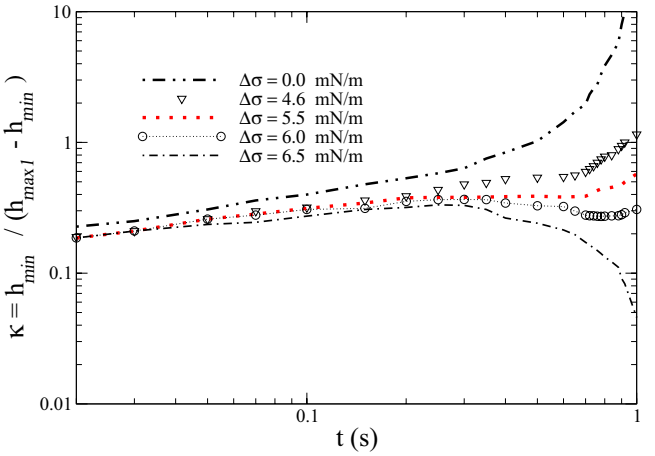

Fig. 5. (Color online) Coalescence coefficient over time for different surface tension gradients. The results are provided by fully three-dimensional phase field simulations.

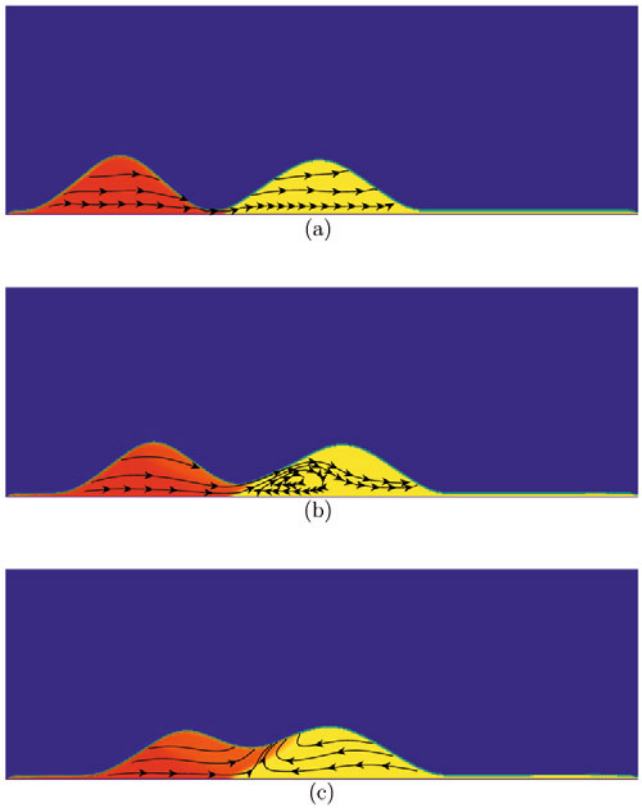

Fig. 4. (Color online) 2D phase field simulations on coalescence of two sessile drops connected through a precursor film, assisted by Marangoni effect at the liquid-gas interface. At $t = 0$ droplet 1 (left-hand side) has a lower surface tension than droplet 2 (right-hand side): $\sigma_1 = 0.05\,\mathrm{N/m}$, $\Delta\sigma = 5\,\mathrm{mN/m}$. The snapshots correspond to: (a) $t = 0.4\,\mathrm{s}$; (b) $t = 0.8\,\mathrm{s}$; (c) $t = 1.1\,\mathrm{s}$. Concentration and flow fields during coalescence can be visualized at different times.

occurs along the droplet interface, continued with a vortex ring (a swirling flow) in the droplet with higher surface tension. The mixing process is well visible in fig. 4, first at the drop surface—driven by Marangoni forces—and, later in the entire drop volume due to diffusion/convection phenomena.

Comparing with the experimental results from [13], the shapes from fig. 3 are qualitatively the same. The minimum of κ is reached for $t \approx 0.4\,\mathrm{s}$ and the minimal difference in surface tension necessary to achieve a temporary separation of the droplets is $\Delta\sigma = 3.3\,\mathrm{mN/m}$. That means a good agreement with the experiment. But a stronger intermittence at the precursor film is followed by a faster mixture. Moreover, the fusion time—until the minimum between drops disappears and the coalescence coefficient goes to infinity, $\kappa \to \infty$—becomes shorter with the increase of the surface tension gradients between the droplets, a fact which is not observed in experiments.

This aspect will be "corrected" in a three-dimensional description. In two spatial dimensions, the geometry of the contact line between the two drops is an infinite straight line and remains a straight line during the delayed coalescence. Thus, one analyzes in fact the interaction between two infinitely long liquid cylinders. A planar two-dimensional formulation cannot catch the dynamics and the droplet curvature in the transverse direction. For this reason, further simulations are carried out with the full three-dimensional version of our code.

3.2 Three-dimensional results

We assume two liquid drops with the same characteristics as in the previous section. The simulations correspond to a mesh with $660 \times 600 \times 200$ under lateral periodic boundary conditions. The system is closed at the top and at the bottom (with no-slip condition for the velocity field). At the solid substrate we have $\rho_S = 0.925$ corresponding to $\theta = 15°$.

From 3D simulations we have a better agreement with the experiment, see fig. 5. The curves reproduce very well quantitatively the experimental curves presented in [13]. The minimal difference in surface tension necessary to achieve a temporary non-coalescence of droplets

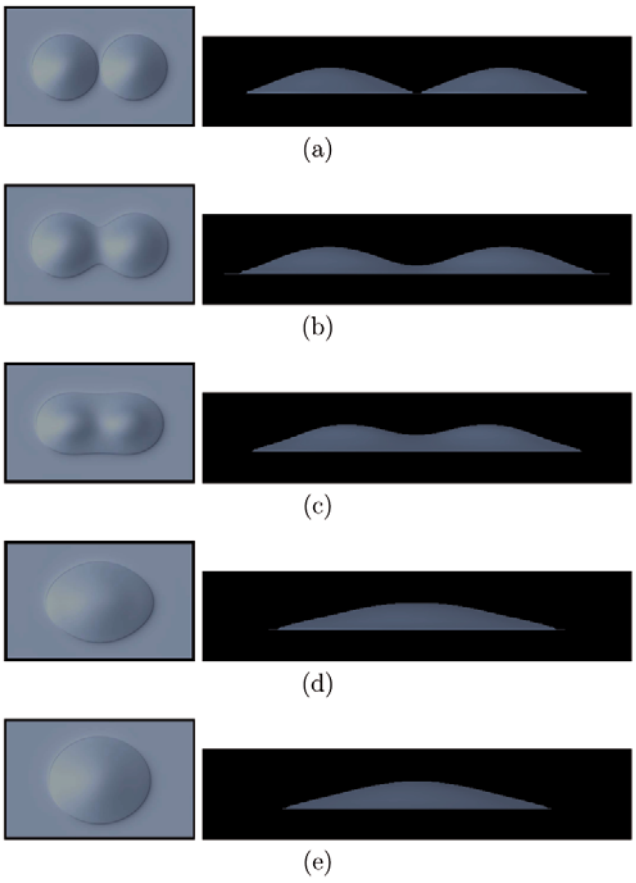

Fig. 6. 3D phase field simulations on coalescence of two identical sessile drops connected through a precursor film. Both liquid droplets have the same surface tension. The snapshots present top and side views of the fusing droplets corresponding to: (a) $t = 0$; (b) $t = 0.15\,\mathrm{s}$; (c) $t = 0.75\,\mathrm{s}$; (d) $t = 1\,\mathrm{s}$; (e) $t = 1.25\,\mathrm{s}$.

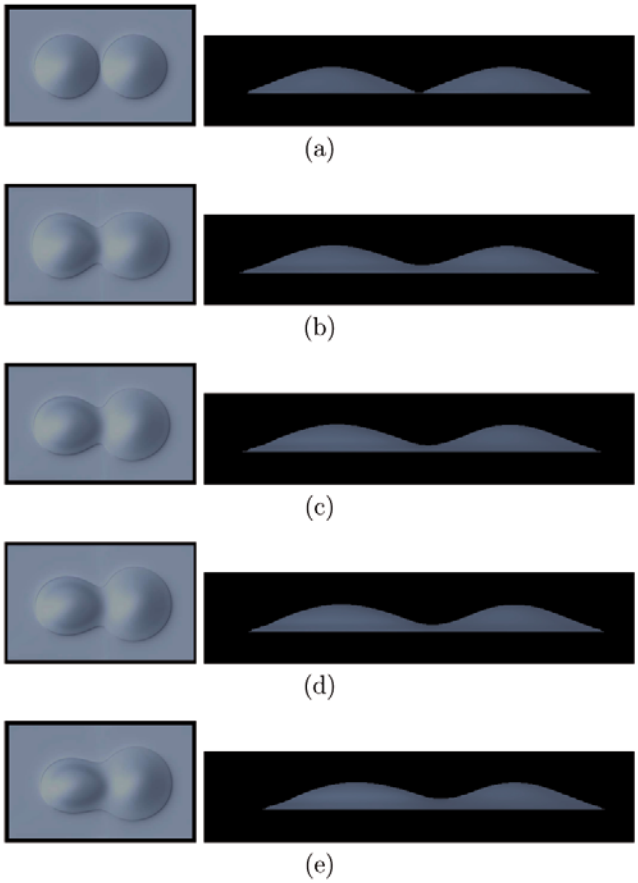

Fig. 7. Time evolution on the coalescence of two drops (top and side views) assisted by Marangoni effect at the liquid-gas interface. The numerical computations are provided by the phase field theory in three-dimensional description with $h(t = 0) = 0.1\,\mathrm{mm}$, $\rho = 10^3\,\mathrm{kg/m^3}$, $\nu = 5 \cdot 10^{-6}\,\mathrm{m^2/s}$, $\sigma_1 = 0.05\,\mathrm{N/m}$, $\Delta\sigma = 6\,\mathrm{mN/m}$, and the contact angles for both liquids are $\theta = 15^\circ$. The snapshots correspond to: (a) $t = 0$; (b) $t = 0.25\,\mathrm{s}$; (c) $t = 0.75\,\mathrm{s}$; (d) $t = 1\,\mathrm{s}$; (e) $t = 1.4\,\mathrm{s}$. The coalescence is intermittent between panels (b) and (d).

is $\Delta\sigma = 5.5\,\mathrm{mN/m}$, *i.e.* by an increase of around 10% of the surface tension absolute value. This result is in excellent agreement with the experiment. In contrast to 2D simulations, 3D simulations describe correctly longer fusion times for larger surface tension differences and catch also a separation of the drops in opposite directions for $\Delta\sigma \geq 6.5\,\mathrm{mN/m}$. For different coalescence regimes, figs. 6, 7 and 8 display representative snapshots with drop profiles—top and side views—for three representative cases. Figure 6 illustrates "fast coalescence" of two identical droplets ($\Delta\sigma = 0$), figs. 7 and 8 show "intermittent coalescence" for $\Delta\sigma = 6.0\,\mathrm{mN/m}$ and $\Delta\sigma = 6.5\,\mathrm{mN/m}$, respectively. In figs. 7 and 8 an intermittence in the growth of the liquid bridge between the interacting drops can be observed after $t \approx 0.3\,\mathrm{s}$. At $t = 1\,\mathrm{s}$ the two identical drops from fig. 6 are already fused, while in figs. 7 and 8 the two liquid droplets are well separated at the same time. For the situation presented in fig. 8, the interruption at the precursor film becomes strong enough to separate the droplets in opposite directions. In this case, the Marangoni driven flow creates vortices not only inside drop 2, but also inside drop 1. The back flows near the substrate inside the droplet 1 (with lower surface tension) leads to a repulsion of the drops. The return flows are difficult to be visualized in three spatial dimensions, but they have been previously illustrated in 2D simulations for delayed coalescence of micro-droplets in confined geometries at larger Reynolds numbers (see fig. 6 from [32]).

We present in the following another interesting phenomenon, characteristic for fully three-dimensional description, which can be observed after the moment of fusion. Figures 9-11 show the time dependence of the drop heights (top view profiles on left columns and side view profiles on right columns) for $\Delta\sigma = 3.4\,\mathrm{mN/m}$, $\Delta\sigma = 4.6\,\mathrm{mN/m}$, and $\Delta\sigma = 6.0\,\mathrm{mN/m}$, respectively. Figures 9 and 10 correspond to a "fast coalescence"—under the classification mentioned above—while fig. 11 corresponds to a "delayed coalescence". For some relevant cases, figs. 9-11 show also the contour lines for the molar fraction $c = 0.5$ at the food of the drops, near the solid substrate. Concentration contour lines permit a better knowledge of the

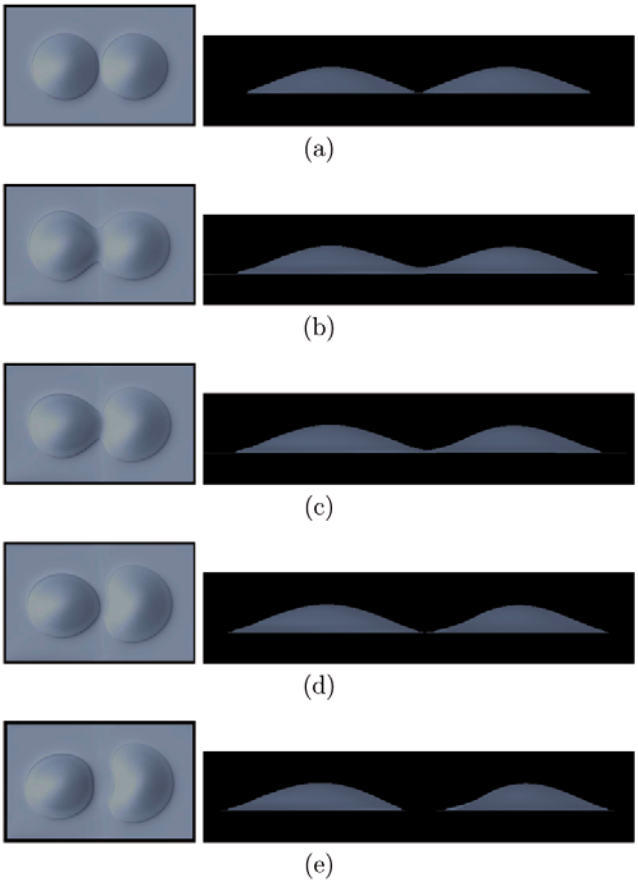

Fig. 8. Same as in fig. 7 for $\Delta\sigma = 6.5\,\mathrm{mN/m}$: (a) $t = 0$; (b) $t = 0.15\,\mathrm{s}$; (c) $t = 0.5\,\mathrm{s}$; (d) $t = 0.65\,\mathrm{s}$; (e) $t = 1.25\,\mathrm{s}$. The interaction via bridging film is completely interrupted after $t \approx 0.6\,\mathrm{s}$ (in our simulations the coalescence is considered "completely interrupted" when $\kappa \leq \kappa(t = 0)/2$).

droplet topology during the coalescence process. Panels (b) and (c) from figs. 9-11 underline the significance of the mixing process in droplet fusion. At $t = 1.25\,\mathrm{s}$ the merging front looks wide in fig. 9 and very narrow and throttled in fig. 11. Figure 10 depicts an intermediary situation for the same time. Component mixing rapidly reduces the surface tension difference and thus promotes fusion. As long as the connecting liquid channel between the droplets remains shallow as in fig. 11-c, the two components mix slowly, keeping the drops temporarily separated from each other.

By fusion of identical droplets ($\Delta\sigma = 0$), the single formed drop quickly relaxes to its equilibrium shape (see fig. 6). For a difference in surface tension of $\Delta\sigma = 3.4\,\mathrm{mN/m}$ (fig. 9), the single formed drop becomes strongly deformed, but no separation of small liquid portions is detected in the long time limit. The situations illustrated in figs. 6 and 9 correspond to a *total coalescence*.

For $\Delta\sigma = 4.6\,\mathrm{mN/m}$ the collision velocity is large enough to produce the rupture of the mother droplet and to leave behind a secondary droplet (fig. 10-d). This effect, called in the literature *partial coalescence*, cannot be observed in two-dimensional approximation because in this geometry the 2D-mixing front remains always straight.

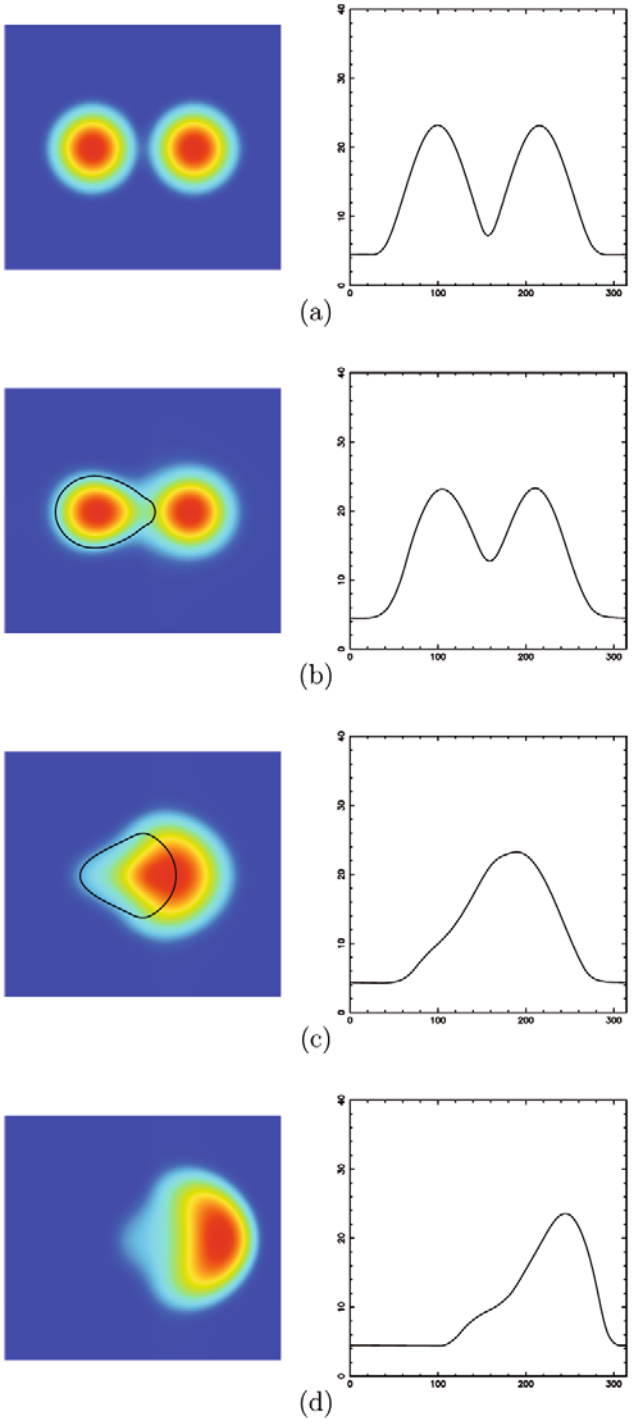

Fig. 9. (Color online) Drop heights (top and side views) at different moments for a difference in surface tension of $\Delta\sigma = 3.4\,\mathrm{mN/m}$ between the drops. The snapshots correspond to: (a) $t = 0$; (b) $t = 0.6\,\mathrm{s}$; (c) $t = 1.25\,\mathrm{s}$; (d) $t = 1.8\,\mathrm{s}$. The contour lines indicated in panels (b) and (c) show the distribution of the molar fraction $c = 0.5$ at the food of the drops, near the solid substrate. In early time coalescence occurs a "fast coalescence", after fusion one observes a strong deformation of the single formed drop.

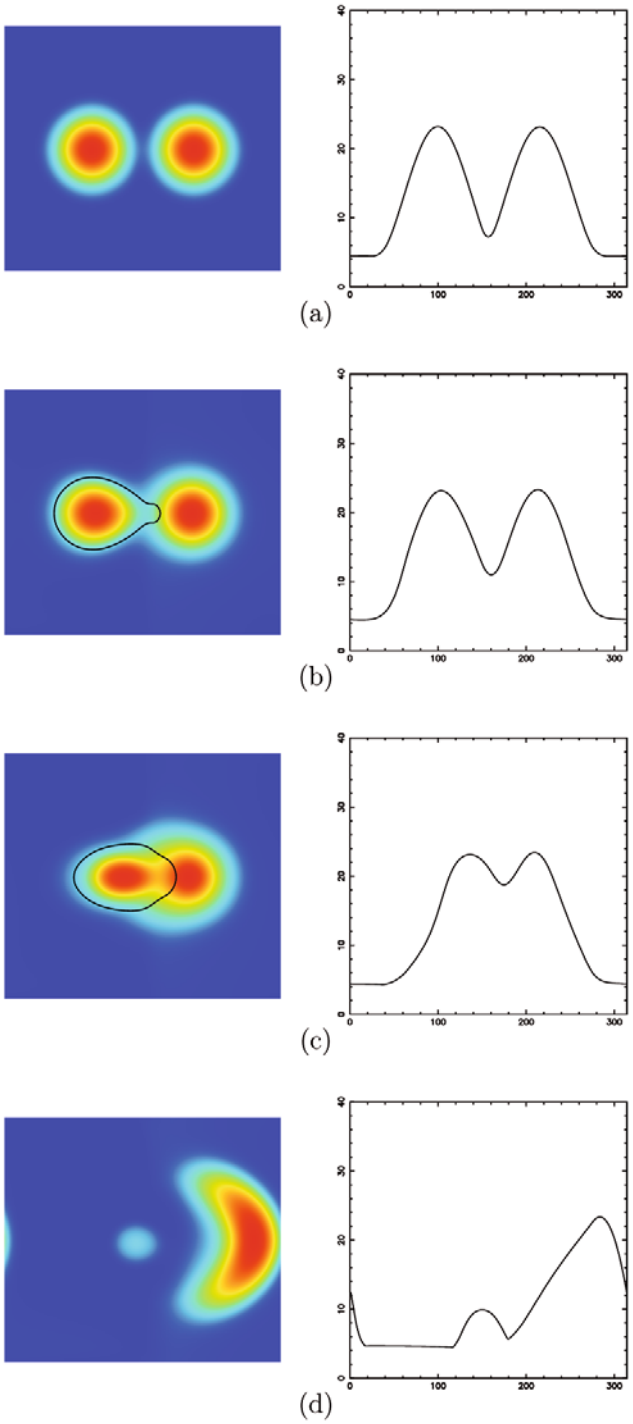

Fig. 10. (Color online) Time evolution of droplet topology (from top and lateral sides) for $\Delta\sigma = 4.6\,\mathrm{mN/m}$. The snapshots correspond to: (a) $t = 0$; (b) $t = 0.6\,\mathrm{s}$; (c) $t = 1.25\,\mathrm{s}$; (d) $t = 2.1\,\mathrm{s}$. Fusion impact velocity is high enough to produce a secondary drop formation in long time evolution.

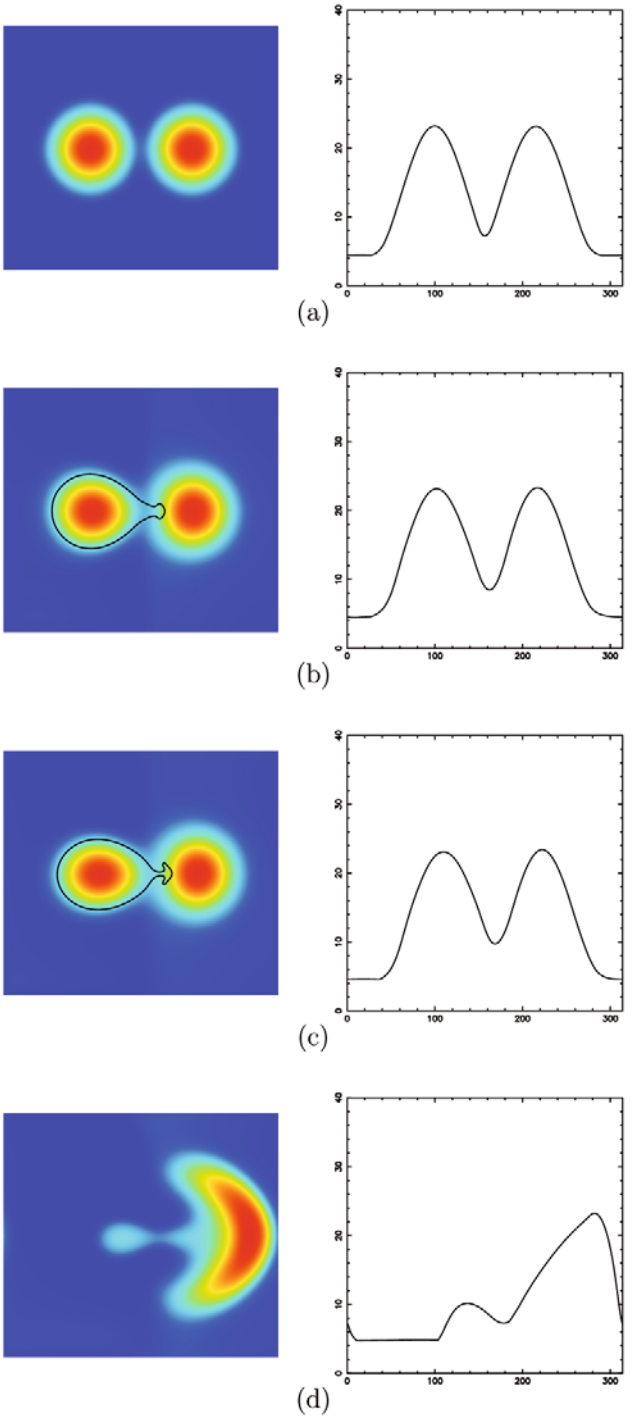

Fig. 11. (Color online) Same as in fig. 10 for $\Delta\sigma = 6.0\,\mathrm{mN/m}$: (a) $t = 0$; (b) $t = 0.6\,\mathrm{s}$; (c) $t = 1.25\,\mathrm{s}$; (d) $t = 2.5\,\mathrm{s}$.

The physical parameters identified of importance in the partial coalescence of a liquid droplet onto a reservoir with the same liquid are the surface tension σ_1, the radius of the drop R, the kinematic viscosity ν and its density ρ. These quantities build, mainly, two dimensionless control parameters: the Ohnesorge number which is the ratio between the capillary time $\sqrt{\rho R^3/\sigma_1}$ and the viscous time R^2/ν

$$Oh = \nu\sqrt{\frac{\rho}{\sigma_1 R}}$$

and the Bond number defined as the square of the ratio between the capillary time $\sqrt{\rho R^3/\sigma_1}$ and the gravity

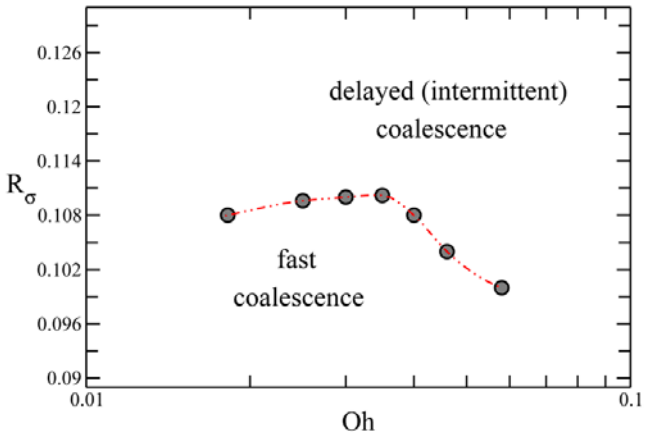

Fig. 12. Phase diagram (Oh, R_σ) illustrating different fusion regimes in early time evolution for the coalescence of two drops consisting of different perfectly miscible liquids sitting on a solid substrate under static contact angles between 10° and 15°.

time $\sqrt{R/g}$

$$Bo = \frac{\rho g R^2}{\sigma_1}$$

(see [5] and references therein).

For *fussing sessile drops having different surface tensions*, the drop dynamics is driven not by gravity forces $\rho g R^3$, but by Marangoni forces $\Delta\sigma R$. In this case the gravity time $\sqrt{R/g}$ will be replaced by the characteristic time of Marangoni effects $\sqrt{\rho R^3/\Delta\sigma}$ and the Bond number will be replaced by the surface tension ratio

$$R_\sigma = \frac{\Delta\sigma}{\sigma_1}\,.$$

For Ohnesorge number we consider in this study $Oh = 0.035$ and for static contact angles at the solid substrate between 10° and 15°, the minimal surface tension ratio necessary to obtain a secondary drop formation is $R_\sigma = 0.09$.

The "fast" and "delayed (intermittent) coalescences" may also be described in terms of Ohnesorge numbers Oh and surface tension ratios R_σ. Thus, for the problem studied in this paper, fig. 12 provides a phase diagram (Oh, R_σ) in which different coalescence regimes in early time evolution can be distinguished, offering in this way an operational criterion for applications.

4 Conclusions

In this paper, we have reported phase field simulations in two and three spatial dimensions on coalescence of sessile droplets consisting of perfectly miscible liquids, sitting on highly wettable solid substrates. A criterion to distinguish between different coalescence regimes in early time evolution was formulated and discussed. Pattern formation, droplet dynamics and concentration distributions during coalescence were investigated in detail.

A comparison between 2D and 3D computer results shows that the third spatial dimension provides a better description closer to experiment. Concentration contour lines provided by 3D numerical simulations prove one more time that Marangoni stresses can prevent for some time the mixing of the two components and produce a delay in drop fusion. The curves obtained numerically in fully three-dimensional formulation are very similar to the experiments and the theoretical critical values are in good agreement.

In fact, there are much differences between 2D and 3D-contact line geometry. The 2D-problem reduces to the interaction of two liquid cylindrical caps. The merging front remains in two-dimensional "picture" always an infinite straight line. A complete description of the problem can be realized only in three dimensions, because, in reality, the merging front becomes curved owing to the flows driven by Marangoni forces. Under certain conditions, after fusion one remarks a secondary drop formation, behind the mother droplet. This is definitely a 3D-effect, emphasized in this paper for the first time for this kind of coalescence.

The authors thank Hans Riegler and Stefan Karpitschka for fruitful discussion on experiments of delayed coalescence. This work was founded by a grant from the Deutsche Forschungsgemeinschaft (DFG), project "Dynamics of interfaces between drops with miscible liquids".

References

1. M. Wu, T. Cubaud, C.-M. Ho, Phys. Fluids **16**, L51 (2004).
2. G.F. Christopher, J. Bergstein, N.B. End, M. Poon, N. Nguyen, S.L. Anna, Lab Chip **9**, 1102 (2009).
3. S.T. Thoroddsen, K. Takehara, Phys. Fluids **12**, 1265 (2000).
4. H. Aryafar, H.P. Kavehpour, Phys. Fluids **18**, 072105 (2006).
5. T. Gilet, K. Mulleners, J.P. Lecomte, N. Vandewalle, S. Dorbolo, Phys. Rev. E **75**, 036303 (2007).
6. F. Blanchette, T.P. Bigioni, J. Fluid Mech. **620**, 333 (2009).
7. D.G.A.L. Aarts, H.N.W. Lekkerkerker, H. Guo, G.H. Wegdam, D. Bonn, Phys. Rev. Lett. **95**, 164503 (2005).
8. W.D. Ristenpart, P.M. McCalla, R.V. Roy, H.A. Stone, Phys. Rev. Lett. **97**, 064501 (2006).
9. N. Kapur, P.H. Gaskell, Phys. Rev. E **75**, 056315 (2007).
10. D.H. Bangham, Z. Saweris, Z. Trans. Faraday Soc. **34**, 554 (1938).
11. H. Riegler, P. Lazar, Langmuir **24**, 6395 (2008).
12. S. Karpitschka, H. Riegler, Langmuir **26**, 11823 (2010).
13. S. Karpitschka, H. Riegler, in preparation (2011).
14. R. Borcia, S. Menzel, M. Bestehorn, S. Karpitschka, H. Riegler, Eur. Phys. J. E **34**, 24 (2011).
15. A.J. Bray, Adv. Phys. **43**, 357 (1994).
16. D. Jasnow, J. Viñals, Phys. Fluids **8**, 660 (1996).
17. D.M. Anderson, G.B. McFadden, A.A. Wheeler, Annu. Rev. Fluid Mech. **30**, 139 (1998).
18. R. Borcia, M. Bestehorn, Phys. Rev. E **67**, 066307 (2003).
19. L.M. Pismen, Y. Pomeau, Phys. Rev. E **62**, 2480 (2000).
20. J.W. Cahn, J.E. Hilliard, J. Chem. Phys. **28**, 258 (1958).

21. D.J. Korteweg, Arch. Sci. Phys. Nat. **6**, 1 (1901).
22. N. Bessonov, J.A. Pojman, V. Volpert, J. Engn. Math. **49**, 321 (2004).
23. B. Zoltowski, Y. Chekanov, J. Masere, J.A. Pojman, V. Volpert, Langmuir **23**, 5522 (2007).
24. N. Bessonov, J. Pojman, G. Viner, V. Volpert, B. Zoltowski, Math. Model. Nat. Phenom. **3**, 108 (2008).
25. P. Colinet, J.C. Legros, M.G. Velarde, *Nonlinear Dynamics of Surface Tension* (Wiley, Berlin, 2001) p. 127.
26. A.A. Nepomnyashchy, M. Velarde, P. Colinet, *Interfacial Phenomena and Convection* (Chapman & Hall/CRC, Boca Raton, FL, 2002) p. 262.
27. C. Hirsch, *Numerical Computation of Internal and External Flows*, Vol. **1** (Wiley, New York, 1998) p. 201.
28. M. Bestehorn, *Hydrodynamik und Strukturbildung* (Springer-Verlag, Berlin, 2006) p. 347.
29. R. Borcia, M. Bestehorn, Phys. Rev. E **75**, 056309 (2007).
30. R. Borcia, I.D. Borcia, M. Bestehorn, Phys. Rev. E **78**, 066307 (2008).
31. R. Borcia, I.D. Borcia, M. Bestehorn, Eur. Phys. J. ST **166**, 127 (2009).
32. R. Borcia, M. Bestehorn, Phys. Rev. E **82**, 036312 (2010).